The electronic structure of polyhex carbon tori

A. Ceulemans, L. F. Chibotaru, S. A. Bovin, and P. W. Fowler

Citation: The Journal of Chemical Physics **112**, 4271 (2000); doi: 10.1063/1.480972
View online: http://dx.doi.org/10.1063/1.480972
View Table of Contents: http://scitation.aip.org/content/aip/journal/jcp/112/9?ver=pdfcov
Published by the AIP Publishing

The electronic structure of polyhex carbon tori

A. Ceulemans, L. F. Chibotaru, and S. A. Bovin
Department of Chemistry, University of Leuven, Celestijnenlaan 200F, B-3001 Leuven, Belgium

P. W. Fowler
School of Chemistry, University of Exeter, Stocker Road, Exeter EX4 4QD, United Kingdom

(Received 13 July 1999; accepted 2 December 1999)

The π-orbital electronic structure of polyhex carbon tori constructed from bent individual single-wall nanotubes is investigated within the tight-binding approach. Analytical solutions for tori from nanotubes of arbitrary radius, length, chirality, and twisting angle are derived using simple geometrical and band-structure arguments. Vanishing of the gap between highest occupied and lowest unoccupied molecular orbitals for a torus imposes divisibility by 3 on the indices of chiral and twisting vectors, which translates into one graph-theoretical condition: a metallic polyhex torus is constructible as a leapfrog transformation of a smaller polyhex torus. © *2000 American Institute of Physics.* [S0021-9606(00)70408-9]

I. INTRODUCTION

Carbon nanotubes can be organized to form circular structures,[1–3] though whether as perfect tori[1] or coiled ropes of single-walled carbon nanotubes (SWCN)[3] is under debate. Nevertheless, toroidal carbon structures are topologically possible, and are local minima on the potential surface.[4,5] Proposals for toroidal structures were made soon after the discovery of carbon nanotubes in 1991 (Ref. 6) and it was suggested that strain energy could be reduced by inserting equal numbers of pentagonal and heptagonal defects along external and internal equatorial circuits, respectively.[4,7] The resulting tori would be polygonal if the number of defects is small, and early members of the series have radii of curvature down to a few nanometers.[5,8,9] Pentagon–heptagon tori can be given a more circular appearance by incorporation of a sufficient number of nonhexagonal rings. Circular ''polyhex'' tori can be obtained by uniform buckling of a sufficiently large single nanotube and connection of its two ends.[10] These ''elastic'' tori can form locally stable structures only beyond a critical radius of curvature, when the gain of covalent energy from the saturation of dangling bonds of the open nanotube exceeds the strain induced by the bending. A simple estimate of these two energies shows that the critical radius of an elastic torus made from a (10,10) nanotube is approximately 100 nm,[9] close to the limit found in experiment.

As prototypes of molecular nanoscale rings, toroidal nanotubes have recently attracted attention in connection with their magnetic properties. In addition to the well understood large diamagnetic response that scales with ring area,[8,9] a purely ''toroidal'' property, the anapole magnetic moment, is predicted.[11] Aharonov–Bohm oscillations of electronic structure[12] and persistent currents[13] in toroidal carbon nanotubes have also been investigated theoretically.

Although less favorable energetically for small diameters, polyhex tori resemble (in size and shape) the observed circular ropes. Kirby *et al.*[10] published a seminal article which addressed the eigenvalue problem in polyhex tori, and gave a partial analytical solution in terms of a canonical construction of tori from patches of the graphite sheet. Later investigations, employing the concept of reciprocal space, were limited to tori from untwisted nanotubes containing an integer number of translational units.[9,12] However, the nanotubes in a rope are often observed to be twisted. [To avoid confusion in the case when nanotubes have intrinsic chirality (as do all tubes apart from the special ''armchair'' and ''zigzag'' classes),[14] note that ''twist'' here means an additional physical distortion caused by external forces.] Such twists have important topological consequences for toroidal nanotubes since the process of construction can (and sometimes *must*) introduce an offset at the place where the two ends meet. Any tube can close into a torus if supplied with an appropriate twist in this sense.

In the present article the π-orbital electronic structure of polyhex carbon tori of fully general form is investigated within the tight-binding approximation. The analytical solution for the spectrum will be described in terms of the mapping of the carbon network of a torus onto the graphite lattice. The zone-folding procedure used earlier for SWCN[14] is first reviewed (Sec. II) and then adapted to the toroidal case (Sec. III). Connections between the zone-folding picture and regularities in the spectrum are established (Sec. IV) and used to derive a criterion for metallicity (Sec. V). A specific example is given in Sec. VI. Finally, Sec. VII discusses further generalizations and conclusions.

II. π-ELECTRON STATES OF AN INFINITE SINGLE-WALLED CARBON NANOTUBE

Consider the infinite graphite sheet. It can be generated by applying translations, $\boldsymbol{t}=n\boldsymbol{a_1}+m\boldsymbol{a_2}$, where n and m are integers and $\boldsymbol{a_1}$ and $\boldsymbol{a_2}$ are unit vectors, to a unit cell that contains two carbon atoms joined by a bond of length r_{CC} [Fig. 1(a)]. The reciprocal lattice is constructed with unit vectors $\boldsymbol{b_1}$ and $\boldsymbol{b_2}$, derived from $\boldsymbol{a_1}$ and $\boldsymbol{a_2}$ in the standard way.[15,16] In the Cartesian (x,y) coordinate system of Fig. 1(a) these vectors are given by

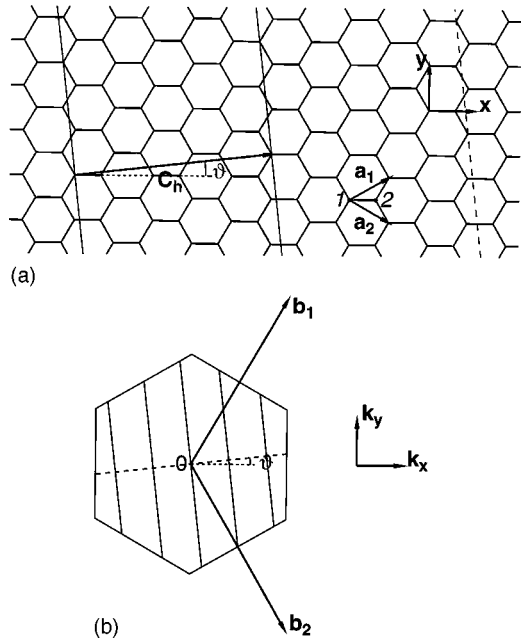

FIG. 1. (a) $\boldsymbol{a}_1$ and $\boldsymbol{a}_2$ are unit vectors and bold sites **1** and **2** denote two carbon atoms of the graphite's unit cell. The fine line delineates the strip corresponding to an unrolled (3,2) nanotube and the dashed line shows its periodic repetition. (b) The first Brillouin zone of a graphite sheet. $\boldsymbol{b}_1$ and $\boldsymbol{b}_2$ are unit vectors of the reciprocal lattice corresponding to $\boldsymbol{a}_1$ and $\boldsymbol{a}_2$. Parallel lines correspond to ''allowed'' $\boldsymbol{k}$-states in a (3,2) nanotube.

$$\begin{aligned}
\boldsymbol{a}_1 &= a\left(\frac{\sqrt{3}}{2}, \frac{1}{2}\right),\\
\boldsymbol{a}_2 &= a\left(\frac{\sqrt{3}}{2}, -\frac{1}{2}\right),\\
\boldsymbol{b}_1 &= \frac{2\pi}{a}\left(\frac{1}{\sqrt{3}}, 1\right),\\
\boldsymbol{b}_2 &= \frac{2\pi}{a}\left(\frac{1}{\sqrt{3}}, -1\right),
\end{aligned} \tag{1}$$

where $a = a_1 = a_2 = \sqrt{3} r_{CC} \approx 1.42 \times \sqrt{3}$ Å. The unit cell in reciprocal space corresponds to the first Brillouin zone which, by the Wigner–Seitz construction,[15,16] is a regular hexagon [Fig. 1(b)]. The vectors confined by this zone [the $\boldsymbol{k}$ vectors (k_x, k_y)] correspond to irreducible representations of the translation group of the graphite lattice with

$$\begin{aligned}
-\frac{2\pi}{\sqrt{3}a} &< k_x \leqslant \frac{2\pi}{\sqrt{3}a},\\
-\frac{4\pi}{3a} &< k_y \leqslant \frac{4\pi}{3a}.
\end{aligned} \tag{2}$$

The π-electron orbitals are carbon $2p_z$ orbitals projecting perpendicularly from the plane of the sheet. Within the tight-binding approximation, the π-electron band structure is a textbook example[17] but must be revisited briefly since it forms the basis for the subsequent toroidal case. The π-electron wave functions that correspond to an irreducible representation $\boldsymbol{k}$ of the translation group (the band orbitals) are

$$|\mu \boldsymbol{k}\rangle = c^1_{\mu \boldsymbol{k}} |\boldsymbol{k}\rangle_1 + c^2_{\mu \boldsymbol{k}} |\boldsymbol{k}\rangle_2, \tag{3}$$

where

$$\begin{aligned}
|\boldsymbol{k}\rangle_1 &= \frac{1}{\sqrt{N}} \sum_{\boldsymbol{t}} e^{i\boldsymbol{k}\boldsymbol{t}} |\boldsymbol{t}\rangle_1,\\
|\boldsymbol{k}\rangle_2 &= \frac{1}{\sqrt{N}} \sum_{\boldsymbol{t}} e^{i\boldsymbol{k}\boldsymbol{t}} |\boldsymbol{t}\rangle_2,
\end{aligned} \tag{4}$$

N is the number of unit cells, μ is an index distinguishing the two bands, $|\boldsymbol{t}\rangle_\nu$ ($\nu = 1,2$) is a $2p_z$ orbital centered on atom ν of the unit cell $\boldsymbol{t}$, and $c^1_{\mu \boldsymbol{k}}$ and $c^2_{\mu \boldsymbol{k}}$ are mixing coefficients.

These coefficients and the corresponding eigenvalues $E_{\mu \boldsymbol{k}}$ (the band energies) are found by diagonalizing 2×2 blocks of the tight-binding matrix

$$\begin{array}{c} \\ {}_1\langle \boldsymbol{k}| \\ {}_2\langle \boldsymbol{k}| \end{array} \begin{array}{c} \begin{array}{cc} |\boldsymbol{k}\rangle_1 & |\boldsymbol{k}\rangle_2 \end{array} \\ \begin{pmatrix} \alpha & h_{\boldsymbol{k}}\beta \\ h^*_{\boldsymbol{k}}\beta & \alpha \end{pmatrix} \end{array}, \tag{5}$$

where α is the energy of the electron in a noninteracting $2p_z$ atomic orbital, β is the transfer integral between nearest-neighbor $2p_z$ orbitals on directly bonded atoms separated by r_{CC}, and $h_{\boldsymbol{k}}$ is the $\boldsymbol{k}$-dependent dimensionless integral

$$h_{\boldsymbol{k}} = (1 + 2e^{-ik_x a\sqrt{3}/2} \cos(k_y a/2)). \tag{6}$$

As in simple Hückel theory of molecular π-systems, the energies are most naturally defined on a scale with α as origin and β as unit. Diagonalization of (5) then gives

$$E_{\mu \boldsymbol{k}} = \alpha + \lambda_{\mu \boldsymbol{k}} \beta, \tag{7}$$

with

$$\lambda_{\mu \boldsymbol{k}} = \pm \left(1 + 4 \cos\frac{k_y a}{2} \cos\frac{\sqrt{3} k_x a}{2} + 4 \cos^2\frac{k_y a}{2}\right)^{1/2}. \tag{8}$$

The eigenvector coefficients are

$$\begin{aligned}
c^1_{\mu \boldsymbol{k}} &= \pm \frac{1}{\sqrt{2}} \frac{h_{\boldsymbol{k}}}{|h_{\boldsymbol{k}}|},\\
c^2_{\mu \boldsymbol{k}} &= \frac{1}{\sqrt{2}}.
\end{aligned} \tag{9}$$

In Eq. (8) the signs refer to the two different bands ($\pm$ for $\mu = 1,2$) and the band energies for a given $\boldsymbol{k}$ are symmetric with respect to the zero of the energy, as eigenvalues of a bipartite graph. For graphite, *every* point (k_x, k_y) within the Brillouin zone corresponds to an allowed pair of band energies and orbitals.

The electronic structure of a general single-walled nanotube is obtained by introducing appropriate boundary conditions, determined by the geometric relation of the tube and the infinite sheet: if a nanotube is cut parallel to its long axis and unrolled, a strip of graphite is obtained [Fig. 1(a)]. The chiral vector $\boldsymbol{C_h}$,[14] perpendicular to the axis of the tube, shows how the edges of the strip are to be connected in the

nanotube. A rotation by 2π of the nanotube around its axis corresponds to translation of the strip by $\boldsymbol{C_h}$ on the sheet. In other words, the graphite sheet is tessellated by periodic repetitions of the strip, implying that the π-orbitals of the nanotube coincide with the band-orbitals of the graphite sheet that are periodic with respect to translations by the chiral vector. It follows from Eq. (3) that the latter condition is obeyed if

$$\boldsymbol{C_h}\cdot\boldsymbol{k}=C_h k_C=2\pi l_n, \tag{10}$$

where l_n is an integer, the *nanotube line index*. The dashed line in Fig. 1(b) shows the direction of $\boldsymbol{k_C}$: it makes the same angle $\theta=\arctan((n-m)/\sqrt{3}(n+m))$ as the vector $\boldsymbol{C_h}=(n,m)$ does with the x-direction. As there are no additional restrictions on components perpendicular to $\boldsymbol{C_h}$, the $\boldsymbol{k}$ vectors relevant to the nanotube are therefore given by parallel straight lines, perpendicular to the dashed line and intersecting it in points spaced by $2\pi/(n^2+m^2+nm)^{1/2}$, according to Eq. (10). Since $\boldsymbol{k}=\boldsymbol{0}$ satisfies this equation, one of the lines will pass through the origin of the Brillouin zone. The electronic structure is thus described by the same solutions as in the case of graphite. However, now the summation in Eq. (3) runs over unit cells of the periodic nanotube confined by the boundaries of the strip [Fig. 1(a)] and the normalization factor corresponds to the number of these unit cells. The procedure as described is a version of the zone-folding technique already applied to nanotubes.[18–20]

It should be pointed out that the present treatment neglects the influence of distortions of the carbon network on the transfer integrals, which in principle are subject to σ/π interaction induced by curvature, physical twisting, etc. In the π-only tight-binding approximation, only the graph of connections is considered, and all energies are functions of the eigenvalues of its (infinite) adjacency matrix. This topological level of approximation reproduces the main details of the electronic density of states in nanotubes.[21] In the next section we will use the same approximation for the treatment of polyhex carbon tori.

III. π-ORBITALS ELECTRONIC STRUCTURE OF POLYHEX CARBON TORI

Polyhex tori can be considered as deriving from finite segments of single-walled nanotubes, cut by a pair of planes perpendicular to the long axis and then reconnected. Ultimately the tori derive from the hexagonal graphite sheet by a process of cutting and pasting. Several constructions appear in the mathematical and chemical literature (e.g., Refs. 10, 22, 23) and all rely on the equivalence of the surface of the torus to a planar parallelogram whose opposite edges have been identified (Scheme I).

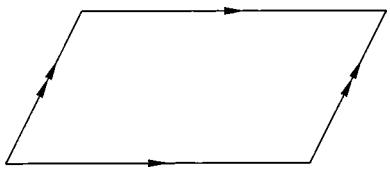

The naive construction used below takes a parallelogram-shaped patch of hexagons defined by two general lattice vectors, and thus appears to require four independent integer parameters; in fact, the patch can always be chosen in such a way as to make one of the four integers vanish. One scheme for doing this is elaborated by Kirby *et al.*[10] An equivalent scheme with a rigorous canonicalization procedure is given by Negami.[22]

Negami works with the dual of the graphite lattice, the equilateral triangulation of the plane, but in terms of the hexagonal lattice his coding of the polyhex torus $T(p,q,r)$ can be stated as follows: draw a parallelogram with corners at hexagon centers and adjacent edges $p\boldsymbol{a_1}$, $r\boldsymbol{a_2}$ parallel to the basis vectors $\boldsymbol{a_1}$, $\boldsymbol{a_2}$, respectively; roll up to form a cylinder with its axis parallel to $\boldsymbol{a_1}$ by identifying points $\alpha\boldsymbol{a_1}$ and $\alpha\boldsymbol{a_1}+r\boldsymbol{a_2}$; now glue the ends of the cylinder but *with an offset*, $0\leqslant q<p$, so that the boundary point $\beta\boldsymbol{a_2}$ is identified with $p\boldsymbol{a_1}+\beta'\boldsymbol{a_2}$ where $\beta-\beta'\equiv q(\mathrm{mod}\,p)$. Reversing the process, any given polyhex torus can be assigned up to six different sets of parameters, depending on the way the cuts are chosen, but all reduce to a canonical code on application of simple modular arithmetic. In the construction devised by Kirby *et al.*, a general angle is allowed between the $\boldsymbol{a_1}$ edge and its neighbor, and a number of subsidiary conditions for canonicalization are proposed.[10] For the present purpose it is easier to work in the redundant four-parameter representation where opposite edges are joined smoothly without any offset. The equivalent Negami or Kirby code can always be found.

Figure 2 introduces the notation by showing three polyhex tori, (a)–(c), peeled and flattened out onto the graphite sheet. As previously, $\boldsymbol{C_h}$ denotes the *chiral vector* connecting the opposite edges of the strip for assembly into a piece of nanotube. The vector $\boldsymbol{T}$ shows how opposite circular edges of this nanotube are to be glued to make the torus. Three cases are shown in order of increasing complexity. In Fig. 2(a) the vector $\boldsymbol{T}$ is perpendicular to $\boldsymbol{C_h}$ as in the case of a normal, i.e., untwisted, nanotube. In Fig. 2(b) we have taken the same piece of nanotube but performed a uniform twist over 2π before pasting the open ends together. As a result in this case $\boldsymbol{T}$ makes an angle different from $\pi/2$ with $\boldsymbol{C_h}$. Figure 2(c) is the most general case in that $\boldsymbol{T}$ addresses a fully arbitrary point (p,q) in the lattice.

The vector $\boldsymbol{C_h}$ defines the chiral angle of a nanotube[14] as the angle it makes with the axis x in Fig. 1(a). In exactly the same fashion the vector $\boldsymbol{T}$ defines the twisting angle for a uniformly twisted nanotube as the angle it makes with the normal to $\boldsymbol{C_h}$, shown by the dashed lines in Fig. 2(b). It is appropriate, therefore, to call the vector $\boldsymbol{T}$ in polyhex tori the *twist vector*. The angle of twist, α, in Fig. 2(c) is related to the vectors $\boldsymbol{C_h}=(n,m)$ and $\boldsymbol{T}=(p,q)$ as follows:

$$\alpha=-\arcsin\left\{\frac{1}{2}\,\frac{m(p+2q)+n(q+2p)}{[(n^2+nm+m^2)(p^2+pq+q^2)]^{1/2}}\right\}. \tag{11}$$

Of course, the roles of twist and chiral vectors can be exchanged for any given parallelogram by swapping the order of assembly of the torus, but α is invariant to this.

The π-orbital electronic structure of polyhex carbon tori can be found following the same line of argument applied for nanotubes in the previous section. Rotation of the finite piece of nanotube (before bending into a torus) by 2π around the axis of the tubule corresponds to translation of the strip on the graphite plane by the vector $\boldsymbol{C_h}$. The rotation of the torus

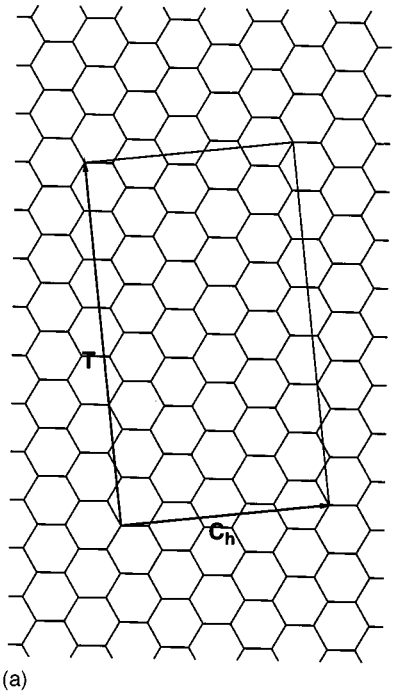

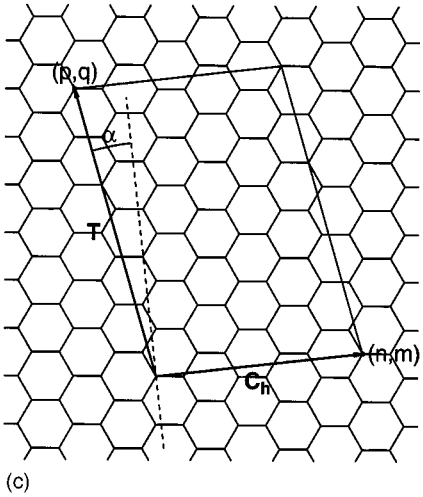

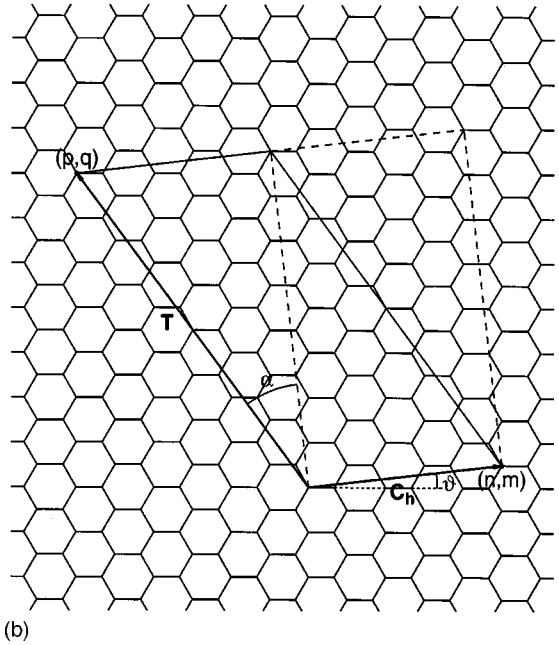

FIG. 2. Strips corresponding to normal (a) and uniformly twisted (b) tori made of a (3,2) nanotube containing one translational unit. The angle of the twist corresponds to a rotation of 2π per translational unit. (c) A general case of a torus built from a (3,2) nanotube with an arbitrary angle of the twist (corresponding to an arbitrary vector $\boldsymbol{T}$).

around its main axis by 2π corresponds to translation by the vector $\boldsymbol{T}$. The graphite plane can therefore be tessellated with periodic repetitions of this strip. Those band orbitals of the graphite sheet that are periodic with respect to translations by $\boldsymbol{C_h}$ and $\boldsymbol{T}$ will be eigenstates of the strip and, at the topological level of the tight-binding approximation, of the corresponding torus as well. Periodicity with respect to the chiral vector will impose the same quantization condition for k_C as in the case of nanotubes, Eq. (10), and hence the same zone-folding picture (Fig. 3) as for the nanotube parent of the torus [Fig. 1(b)] i.e., a set of parallel lines intersecting the dashed line (which indicates the direction of the chiral vector) at 90°. The periodicity with respect to the twisting vector is

$$\boldsymbol{T}\cdot\boldsymbol{k} = T\,k_T = 2\pi\,l_t\,, \tag{12}$$

where l_t is an integer, the *torus line index*. The direction of $\boldsymbol{T}$ is shown by a dotted line in Fig. 3; by definition this line makes a twisting angle α with the normal to the dashed line that specifies $\boldsymbol{C_h}$. Condition (12) defines a set of parallel straight lines, perpendicular to the dashed line and intersecting it in points spaced by $2\pi/(p^2+pq+q^2)^{1/2}$. The value $\boldsymbol{k}=\boldsymbol{0}$ always satisfies this condition, and hence one line will pass through the center of the Brillouin zone. Taken together, the two quantization conditions (10) and (12) give the $\boldsymbol{k}$-points corresponding to π-orbital eigenstates of the polyhex torus as all points of intersection of the two sets of lines occuring within the first Brillouin zone of the graphite sheet.

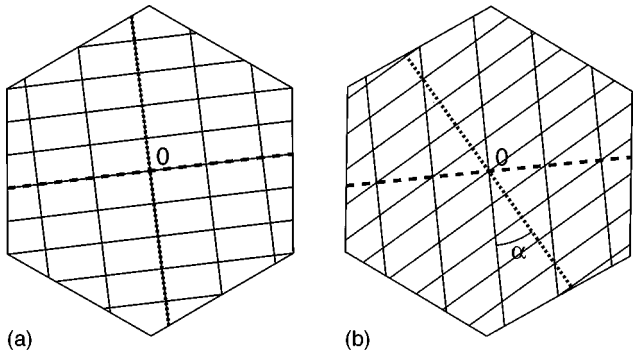

FIG. 3. Wavevectors characterizing the π-orbital eigenstates of two tori, specified in Fig. 2 [(a) and (b), respectively], corresponding to nodes of the network obtained from two sets of parallel lines (see the text).

The approach described above is a generalization of the zone-folding technique previously applied to nanotubes. In the case of tori it corresponds to a double folding of the Brillouin zone of the graphite sheet and allows all relevant $\boldsymbol{k}$-points to be found by a simple geometrical construction (Fig. 3). An immediate result is the conclusion that the twisting inherent in linking the nanotube ends introduces no major complications. Its manifestation is only in the nonorthogonality of the grid in $\boldsymbol{k}$ space. The two sets of lines used in this construction are numbered by corresponding integers on the right hand sides of Eqs. (10) and (12), i.e., l_n for the nanotube lines (perpendicular to the dashed line) and l_t for the torus lines (perpendicular to the dotted line). Therefore the relevant $\boldsymbol{k}$-points can be numbered as (l_n, l_t) provided the intersection point of the lines is found within the first Brillouin zone of the graphite sheet. The vectors $\boldsymbol{C_h}$ and $\boldsymbol{T}$ define the positive direction on dashed and dotted lines, respectively.

The coordinates of a point in Fig. 1(b) are expressed through $(\boldsymbol{a_1}, \boldsymbol{a_2})$ components of the chiral (n,m) and twist (p,q) vectors as follows:

$$k_x = \frac{2\pi}{\sqrt{3}a}\,\frac{l_t(m-n)+l_n(p-q)}{mp-nq},$$
$$k_y = \frac{2\pi}{a}\,\frac{l_t(n+m)-l_n(p+q)}{mp-nq}. \tag{13}$$

The number of $\boldsymbol{k}$-points relevant for the torus is equal to the number of unit cells (hexagons) of the graphite sheet confined by the corresponding strip. It is easily seen that each $\boldsymbol{k}$-point corresponds to one cell of the doubly folded Brillouin zone in Fig. 3. The area of such a cell (in reciprocal space), S_{cell}, is related to the are of the strip, $S_{\text{strip}} = (p(n+\sqrt{3}m/2)+q(m+\sqrt{3}n/2))a^2$, by the equation $S_{\text{cell}} = 4\pi^2/S_{\text{strip}}$. Moreover, by construction each cell is geometrically similar to the strip. Thus one can propose simple rules to construct the double zone-folding picture of Fig. 3:

(i) take the reciprocals of the edge lengths of the strip in Fig. 2, multiply by 2π, and rotate the obtained parallelogram by $\pi/2$;
(ii) tessellate the first Brillouin zone of the graphite sheet with the new cell.

The double zone-folding picture remains the same if we change the order of the two operations used to construct the torus from the strip. Indeed, considering $\boldsymbol{T}$ as chiral and $\boldsymbol{C_h}$ as twist vector gives the same electronic structure as before. One can generalize the shape of the strip for which the electronic structure is invariant at the topological level of approximation: we may take boundary lines of arbitrary shape, the only condition being that opposite boundaries must superimpose under translation by $\boldsymbol{C_h}$ and $\boldsymbol{T}$ respectively.

A point group symmetry may be defined for a polyhedral graph as the topological symmetry,[24] i.e., the largest possible group realized for an idealized 3D embedding of the graph on the relevant surface. With the extra degree of freedom of rotation of a torus, it is conceivable that more than one subgroup of the automorphism group of the graph may be largest in this sense. There is an additional ambiguity for polyhex tori in the $\boldsymbol{T}$, $\boldsymbol{C_h}$ construction stemming from the freedom of choice of the strip. If in doubt, the Negami code gives a sure way of finding a highly symmetric presentation of the graph. Given the best choice of strip, the shape of the cell defines a point group. Rotational symmetry around the main axis of the torus can exist only if the twist vector $\boldsymbol{T}$ contains a whole number (more than one) of translational units. The number of shortest such units into which $\boldsymbol{T}$ can be divided determines the order of the rotation axis. As all vectors parallel to $\boldsymbol{T}$ are characterized by the same ratio of coordinates, the relation between the vector $\boldsymbol{T}=(p,q)$ and the rotation symmetry of the torus is simple: the order of the rotation axis is equal to the largest common divisor of the numbers p and q. Note that this rotational symmetry is unaffected by any distortions of the hexagons made necessary by the bending and twisting of the nanotube.

IV. SYMMETRY POINTS OF THE TOROIDAL BAND STRUCTURE

For the cases where an explicit formula was known,[10] the application of Eq. (7) with the allowed $\boldsymbol{k}$ set Eq. (13), gives exactly the same result. However, the geometrical nature of the present construction gives a transparent interpretation of several features of the spectra of polyhex tori that can be observed in the earlier partial results. The spectra are bipartite, as all cycles in the graph are even but are also multiple in that every eigenvalue λ apart from $+3, +1, -1, -3$ has an even multiplicity. The eigenvalue zero appears in the spectrum only for a special class of polyhex tori (see below) and then with multiplicity four.

The even multiplicities for $|\lambda| \neq 3$ are explained by noting that the origin of the Brillouin zone corresponds to a center of inversion which connects (l_n, l_t) and $(-l_n, -l_t)$ $\boldsymbol{k}$ points, having the same eigenvalue but complex conjugate eigenstates according to Eq. (9). The last property is rooted in the time-reversal symmetry[15] of the band states from which the eigenstates of the torus are constructed. The point $\lambda = \pm 3$ is at the center of inversion (the Γ-point of the Brillouin zone, Fig. 4) and has real eigenvectors. As noted earlier, this point will always be included. The other exception to the rule of even multiplicity is provided by points having eigenvalues $\lambda = \pm 1$. In an infinite graphene sheet their locus corresponds to the boundary of a hexagon (dashed lines in

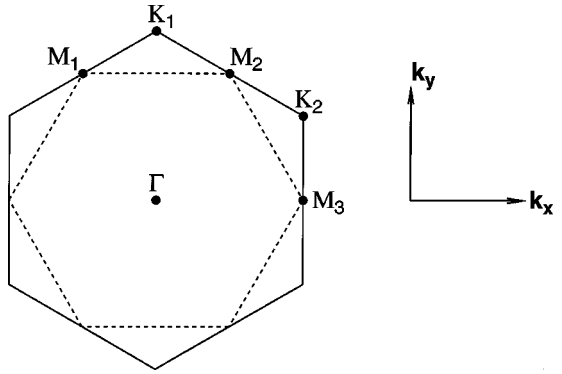

FIG. 4. Symmetry points of the first Brillouin zone of the graphene sheet: $\Gamma(0,0)$; $K_1(0,4\pi/3a)$; $K_2(2\pi/\sqrt{3}a,2\pi/3a)$; $M_1(-\pi/\sqrt{3}a,\pi/a)$; $M_2(\pi/\sqrt{3}a,\pi/a)$; $M_3(2\pi/\sqrt{3}a,0)$. Dashed lines cover all points with eigenvalues ± 1.

Fig. 4) inscribed on the Brillouin zone boundary. Its vertices are the *M*-points of the graphene band structure at midpoints of the edges of the Brillouin zone boundary (Fig. 4). As ***k***-points lying exactly on the boundary of the first Brillouin zone, they will be equivalent and correspond to just a single band state if they differ by a lattice vector of the reciprocal space.[15,16] Thus only three of the six points *M* correspond to distinct ***k*** states (M_1, M_2, and M_3 in Fig. 4). Using Eq. (13) one can express the (l_n,l_t) coordinates of *M*-points through the coordinates of the chiral and twist vectors specifying the torus as follows: M_1-point: $l_t=-q/2$, $l_n=-m/2$, M_2-point: $l_t=p/2$, $l_n=n/2$; M_3-point: $l_t=(p+q)/2$, $l_n=(n+m)/2$. Evidently, a given *M*-point can be an intersection point in the double zone-folding picture if and only if l_t and l_n are integer. This requirement is fulfilled for M_1 if q and m are both even, for M_2 if p and n are both even, and for M_3 if the sums $p+q$ and $n+m$ are even. The conclusion is that none of the *M*-points is intersected when the set $\{n,m,p,q\}$ contains three odd and one even number. In all other cases, an odd number (either one or three) of *M*-points can be intersected.

The multiplicity of the eigenvalues ± 1 in a torus is defined by the number of intersection points lying on the dashed lines in Fig. 4. Apart from the points on the boundary (i.e., *M*-points), the number of these intersections is always even by virtue of the inversion symmetry in ***k***-space. It can also be proved that if the number of allowed *M* points is zero there will be no other intersections with the dashed lines in Fig. 4. Indeed, consider as an example the segment M_1-M_2 parametrized as follows:

$$k_x=\frac{\pi}{\sqrt{3}a}\eta, \quad -1<\eta<1,$$
$$k_y=\frac{\pi}{a}. \tag{14}$$

Substituting the coordinates (14) in Eq. (13), express the (l_n,l_t) coordinates through the coordinates of the chiral and twist vectors and the parameter η. Solving each of these equations for η one obtains

$$\eta=\frac{4l_t+q-p}{p+q},$$
$$\eta=\frac{4l_n+m-n}{n+m}. \tag{15}$$

A necessary condition for some intersection point to lie on the segment M_1-M_2 is provided by simultaneous satisfaction of the two equations in (15) for integer numbers l_t and l_n. This yields

$$2l_t(n+m)-2l_n(p+q)=pm-qn. \tag{16}$$

When the set $\{n,m,p,q\}$ contains three odd numbers and one even the right-hand side of Eq. (16) will be even while the left hand side will be odd. This means that Eq. (16) is never satisfied in this case and, consequently, none of the intersection points can lie on the given segment. But precisely the same is also true for the *M*-points: none of them coincides with an intersection point in the double zone-folding picture.

A similar proof can be provided for other segments of the dashed line in Fig. 4. Hence taking the *M*-points into account, one concludes that eigenvalues ± 1 in a torus are found only with an *odd multiplicity* (see also Ref. 10).

Further symmetry points, the *K*-points in Fig. 4, influence the metallicity of tori, as discussed in the next section.

V. METALLIC POLYHEX TORI

Tight-binding theory makes clear predictions about metallic vs insulating behavior for infinite nanotubes. In the crudest π-only Hückel theory, the metallic tubes are those with indices obeying the Kekulé rule,[25] $2n+m=0 \bmod 3$, and all others have band gaps. In the terminology developed for fullerenes, these metallic tubes are exactly the *leapfrogs*[26] of smaller structures and their zero gap follows from graph-theoretical considerations.[27] More sophisticated treatments that include σ/π interaction predict the opening up of a small gap for the zigzag ($m=0$) members of the leapfrog series, but do not change the prediction of metallic nature for the armchair $n=m$ tubes (which are all leapfrogs). When a nanotube is metallic, it has four exactly nonbonding ***k*** band orbitals, and again this has a simple interpretation in terms of the leapfrog operation.[27] In tight-binding Hückel theory, the metallic nanotubes are exactly the leapfrogs. A similar rule applies to polyhex tori:[27,28] all leapfrog polyhex tori have four nonbonding orbitals and, as the graphs are both even and bipartite, this implies an open shell or ''metallic'' π-configuration. The double zone-folding construction sheds further light on this point, as we now demonstrate.

The intersection points on the lines that define allowed ***k***-states of a polyhex torus depend strongly on ***T*** as Fig. 3 shows, i.e., they are affected by the length and twist of the nanotube from which the torus was constructed. At the Hückel level of treatment, SWCN are metallic when the lines in the zone-folding picture in Fig. 1(b) include the *K*-points of the Brillouin zone (Fig. 4). These are the only points where the two bands of the graphite sheet coincide, i.e., where the energy gap between the occupied and the empty band states disappears. As the points are at corners of the hexagonal Brillouin zone, and hence connected by lattice

vectors, only two of them correspond to nonequivalent $\boldsymbol{k}$-points, shown in Fig. 4 by K_1 and K_2. From the symmetry of the zone-folding picture, it is easily seen that the intersection of one K-point by any line automatically implies intersection of K_1 or K_2 by some other line. In the case of a nanotube, choice of K_1 leads to the following condition for the coordinates of the chiral vector:

$$(n-m)/3=l_n. \tag{17}$$

In the case of a torus this condition is one of two necessary for ''metallicity.'' The second condition is the intersection of the K-point by the torus lines. Again it is enough to check for the K_1-point which yields

$$(p-q)/3=l_t. \tag{18}$$

Thus both $\boldsymbol{T}$ and $\boldsymbol{C_h}$ obey symmetrical Kekulé conditions. Simultaneous divisibility of $(n-m)$ and $(p-q)$ by 3 is equivalent to requiring that the polyhex be a Clar polyhedron[29] and hence a leapfrog of a smaller torus, i.e., that can be derived by omnicapping and dualizing a smaller torus of polyhedral type. Thus the zone-folding argument shows that leapfrog character is the *necessary* and *sufficient* condition for nonbonding orbitals. Interestingly, for *fullerenes*, leapfrog character is a sufficient condition for a *nonzero* HOMO–LUMO gap, i.e., for a molecular ''insulator.'' These opposite consequences of the leapfrog transformation derive from the differences in the cycle structure of the parent graphs.[27]

In the case of a torus, metallicity implies degeneracy and partial occupation of the HOMO orbitals in the neutral molecule. This possibility is expected to give rise to unconventional magnetic properties, such as permanent anapole moments of the toroidal molecules.[11]

VI. AN EXAMPLE

In Fig. 5 we present a simple example that should help to clarify the general method. A torus of 60 atoms has been placed on a simple rectangular patch of the honeycomb lattice with origin at atom 1. $\boldsymbol{C_h}$ runs through atoms 1, 3, 5, 7, 9 and corresponds to the direction of $\boldsymbol{a_1}$; it spans five hexagons, i.e., $\boldsymbol{C_h}=(5,0)$. It makes an angle of 30° with the x-direction. The nanotube line index l_n can take all integer values such that k_C is within the first Brillouin zone:

$$-\frac{4\pi}{3a}<\frac{2\pi l_n}{C_h}\leqslant\frac{4\pi}{3a}. \tag{19}$$

With $C_h=5a$ the allowed values of l_n thus range from -3 to $+3$. As a result seven nanotube lines are perpendicular to the direction of k_C. Similarly the twist vector $\boldsymbol{T}$ runs through atoms 1, 11, 21, 31, 41, 51, and has hexagonal coordinates $\boldsymbol{T}=(3,-6)$. It is perpendicular to the chiral vector. The torus line index l_t is defined by

$$-\frac{2\pi}{\sqrt{3}a}<\frac{2\pi l_t}{T}\leqslant\frac{2\pi}{\sqrt{3}a}, \tag{20}$$

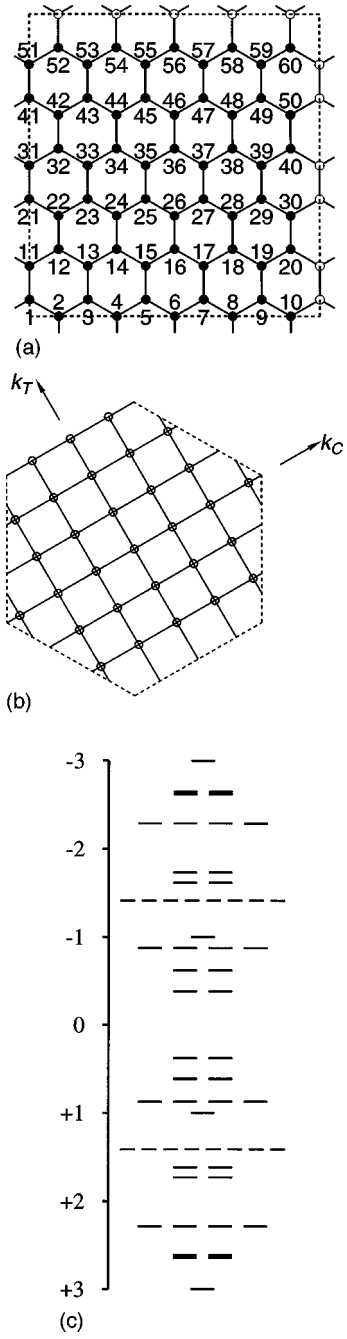

FIG. 5. Example of a 60-atom torus with $(n,m,p,q)=(5,0,3,-6)$: (a) positions of the atoms in the honeycomb plane, (b) allowed lattice points in the Brillouin zone, and (c) eigenvalue spectrum in units of β.

which is the allowed range for k_T. With $T=3\sqrt{3}a$, l_t must lie in the interval $-3<l_t\leqslant+3$. Hence there are six torus lines perpendicular to the direction of k_T. The line for $l_t=+3$ coincides with the zone boundary.

The resulting diagram contains 30 grid points from which eigenvalues and eigenvectors follow by Eqs. (8) and (9). The spectrum shows reflection symmetry and the positive roots are listed in Table I. Note that $l_n=0$, $l_t=3$ coincides with M-points of the hexagonal cell. The corresponding eigenvalue is unity and occurs only once. The eigenvalue $+3$ is at the zone origin and also appears once. All other eigenvalues are at least twofold degenerate.

TABLE I. Positive roots of the eigenvalue spectrum for the torus shown in Fig. 5.

Eigenvalue	Degeneracy
3.0000	1
2.6458	2
2.6180	2
2.2882	4
1.7320	2
1.6180	2
1.4142	8
1.0000	1
0.8740	4
0.6180	2
0.3820	2

VII. GENERALIZATIONS AND CONCLUSIONS

Trivalent polyhex graphs on compact surfaces are possible for two cases: the torus and the Klein bottle. While the problem of self-intersection in 3D renders Klein polyhexes unlikely candidates for stable structures, they have been considered in the chemical literature.[30–32] The spectra of Klein polyhexes are easily disposed of, as every such polyhex is derivable by collapsing in pairs the antipodal points of a centrosymmetric polyhex torus that has twice as many vertices.[30] A similar method can be used for obtaining fullerene-like graphs on the projective plane by collapsing centrosymmetric conventional fullerenes. The g eigenvalues of the polyhex torus yield the spectrum of the adjacency matrix **A** of the Klein polyhex, the u eigenvalues the spectrum of its Hückel Hamiltonian **H**.[30] The two sets differ because of the unavoidable phase interruption in the π-system entailed by the nonorientable nature of the Klein-bottle surface, which distinguishes it from the sphere and torus. For nonbipartite Klein polyhexes, exactly one of the upper and lower band surfaces contributes at any one $\boldsymbol{k}$ point to the spectrum of **A** and the other to **H**, whereas for a bipartite Klein polyhex the $\boldsymbol{k}$-point generates eigenvalues belonging to one and the same spectrum, either of **A** or **H**.[30] The present zone-folding technique therefore also gives the solution to the Klein polyhex spectral problem.

In this article we have extended the zone-folding procedure for the band structure of nanotubes to carbon tori. Polyhex tori are defined by two cyclic boundary conditions on a graphite sheet, giving rise to a two-dimensional grid of allowed $\boldsymbol{k}$-points in the first Brillouin zone. Equivalently, a torus can be defined by joining the ends of a cut nanotube. When the tube must be twisted or offset to make the join, the grid lattice is distorted from rectangular to rhombohedral. The procedure gives a clear pictorial interpretation of the systematics of the π-energy levels of polyhex tori, including the occurrence of open-shell or metallic tori. It is likely that these diagrammatic representations of eigenvalues and eigenvectors in a hexagonal Brillouin zone will prove useful in further studies of isomorphism, symmetry, and enumeration problems for this and related classes of carbon structures.

ACKNOWLEDGMENTS

This research was supported by a grant from the Belgian Government (Programmatie van het Wetenschapsbeleid). P.W.F. acknowledges support from TMR contracts FMRX CT96 0126 and FMRX CT97 0192. The authors thank K. M. Rogers for help in preparing some of the figures.

[1] J. Liu, H. Dai, J. H. Hafner, D. T. Colbert, R. E. Smalley, S. J. Tans, and C. Dekker, Nature (London) **385**, 780 (1997).
[2] T. Vossmeyer *et al.*, Adv. Mater. **10**, 351 (1998), and references therein.
[3] R. Martel, H. R. Shea, and P. Avouris, Nature (London) **398**, 299 (1999).
[4] B. I. Dunlap, Phys. Rev. B **46**, 1933 (1992).
[5] J. C. Greer, S. Itoh, and S. Ihara, Chem. Phys. Lett. **222**, 621 (1994).
[6] S. Iijima, Nature (London) **354**, 56 (1991).
[7] S. Itoh, S. Ihara, and J. I. Kitami, Phys. Rev. B **47**, 1703 (1993).
[8] R. C. Haddon, Nature (London) **388**, 31 (1997).
[9] V. Meunier, Ph. Lambin, and A. A. Lucas, Phys. Rev. B **57**, 14886 (1998).
[10] E. C. Kirby, R. B. Mallion, and P. Pollak, J. Chem. Soc., Faraday Trans. **98**, 1945 (1993).
[11] A. Ceulemans, L. F. Chibotaru, and P. W. Fowler, Phys. Rev. Lett. **80**, 1861 (1998).
[12] M.-F. Lin, R.-B. Chen, and F.-L. Shyu, Solid State Commun. **107**, 227 (1998).
[13] M. F. Lin and D. S. Chuu, Phys. Rev. B **57**, 6731 (1998).
[14] M. S. Dresselhaus, G. Dresselhaus, and P. C. Eklund, *Science of Fullerenes and Carbon Nanotubes* (Academic, New York, 1995).
[15] S. L. Altman, *Band Theory of Solids: An Introduction From the Point of Symmetry* (Clarendon, Oxford, 1994).
[16] J. M. Ziman, *Principles of the Theory of Solids* (Cambridge University Press, Cambridge, 1972).
[17] P. R. Wallace, Phys. Rev. **71**, 622 (1947).
[18] R. Saito, M. Fujita, G. Dresselhaus, and M. S. Dresselhaus, Phys. Rev. B **46**, 1804 (1992).
[19] N. Hamada, S. I. Sawada, and A. Oshiyama, Phys. Rev. Lett. **68**, 1579 (1992).
[20] S. S. Savinskii and N. V. Khokhryakov, JETP **84**, 1131 (1997).
[21] J. W. G. Wildöer, L. C. Venema, A. G. Rinzler, R. E. Smalley, and C. Dekker, Nature (London) **391**, 59 (1998).
[22] S. Negami, Discrete Math. **44**, 161 (1983).
[23] C. Thomassen, Trans. Am. Math. Soc. **323**, 605 (1991).
[24] D. E. Manolopoulos and P. W. Fowler, J. Chem. Phys. **96**, 7603 (1992).
[25] D. J. Klein, W. A. Seitz, and T. G. Schmalz, J. Phys. Chem. **97**, 1231 (1993).
[26] P. W. Fowler and J. I. Steer, J. Chem. Soc. Chem. Commun. **1997**, 1403.
[27] P. W. Fowler and K. M. Rogers, J. Chem. Soc., Faraday Trans. **94**, 2509 (1998).
[28] M. Yoshida, M. Fujita, P. W.Fowler, and E. C. Kirby, J. Chem. Soc., Faraday Trans. **93**, 1037 (1997).
[29] P. W. Fowler and T. Pisanski, J. Chem. Soc., Faraday Trans. **90**, 2865 (1994).
[30] M. Deza, P. W. Fowler, K. M. Rogers, and A. Rassat, J. Chem. Inf. Comp. Sci. (in press).
[31] D. J. Klein, J. Chem. Inf. Comp. Sci. **34**, 453 (1994).
[32] E. C. Kirby, Croat. Chem. Acta **68**, 269 (1995).